Mechanism of action and resistance to Trastuzumab Deruxtecan in patients with metastatic breast cancer: the DAISY trial

Fabrice Andre (fabrice.andre@gustaveroussy.fr)
Institute Gustave Roussy https://orcid.org/0000-0001-5795-8357
Mosele Fernanda
Gustave Roussy https://orcid.org/0000-0001-7841-2900
Elise Deluche
CHU Dupuytren
Amelie LUSQUE
Institut Claudius Regaud
Loic Le-Bescond
Centrale Supélec/Institut Gustave Roussy
Thomas Filleron
Institut Claudius-Regaud
Yoann Pradat
Centrale Supélec
Agnes Ducoulombier
Centre Antoine Lacassagne
Barbara Pistilli
Institut Gustave Roussy
Thomas Bachelot
Centre Léon Bérard
Frederic Viret
Centre Paoli Calmettes
Christelle LEVY
Centre François Baclesse
Nicolas Signolle
Institut Gustave Roussy
Alexia Alfaro
Institut Gustave Roussy
Diep Tran
Institut Gustave Roussy
Ingrid GARBERIS

Institut Gustave Roussy https://orcid.org/0000-0002-0501-8520

Hugues Talbot

Centre de Vision Numérique, Université Paris-Saclay, CentraleSupélec, Inria, 91190 Gif-sur-Yvette

Stergios Christodoulidis

Institut Gustave Roussy https://orcid.org/0000-0002-8773-1070

Maria Vakalopoulou

CentraleSupélec

Nathalie Droin

Gustave roussy https://orcid.org/0000-0002-6099-5324

Aurelie Stourm

Institut Gustave Roussy

Maki Kobayashi

Daiichi Sankyo RD Novare Co., Ltd.

Tomaya Kakegawa

Daiichi Sankyo RD Novare Co., Ltd.

Ludovic Lacroix

Institut Gustave Roussy

Patrick Saulnier

Institut Gustave Roussy

Bastien Job

Institut Gustave Roussy

Marc Deloger

Institut Gustave Roussy

Marta Jimenez

Unicancer https://orcid.org/0000-0002-4233-8478

Vianney Baris

Institut Gustave Roussy

Pierre Laplante

Institut Gustave Roussy

Patricia Kannouche

French National Centre for Scientific Research https://orcid.org/0000-0002-6050-3457

Virginie Marty

Gustave Roussy Cancer Centre

Magali Lacroix-Triki

Institut Gustave Roussy https://orcid.org/0000-0002-6641-8536

Veronique Dieras

Centre Eugène Marquis

Article

Keywords:

Posted Date: September 26th, 2022

DOI: https://doi.org/10.21203/rs.3.rs-2083650/v1

Version of Record: A version of this preprint was published at Nature Medicine on July 24th, 2023. See the published version at https://doi.org/10.1038/s41591-023-02478-2.

Abstract

Trastuzumab deruxtecan (T-DXd) is an anti-HER2 (human epidermal growth factor receptor 2) antibody-drug conjugate which has previously shown efficacy in patients with HER2-overexpressing and HER2-low metastatic breast cancer (mBC). However, the mechanisms of action and resistance of this drug remain partially unclear. DAISY (NCT04132960) is a phase II, open-label study that included patients with mBC whose disease progressed after at least one line of chemotherapy in the metastatic setting. Patients were enrolled in three cohorts according to HER2 expression determined by immunohistochemistry (IHC); cohort 1: HER2-overexpressing (HER2 IHC 3 + or HER2 IHC 2+/ISH+, $n = 72$), cohort 2: HER2-low (HER2 IHC2+/ISH- or HER2 IHC 1+, $n = 74$), and cohort 3: HER2 IHC 0 mBC ($n = 40$). Patients were treated with T-DXd 5.4 mg/kg every 3 weeks until disease progression or unacceptable toxicity. In the full analysis set population ($n = 177$), the confirmed objective response rate (ORR) was of 70.6% (95% CI: 58.3–81) in cohort 1, 37.5% (95% CI: 26.4–49.7) in cohort 2, and 29.7% (95% CI: 15.9–47) in cohort 3 ($p < 0.0001$). The median progression-free survival (PFS) was 11.1 months (95% CI: 8.5–14.4) in cohort 1, 6.7 months (95% CI: 4.4–8.3) in cohort 2, and 4.2 months (95% CI: 2-5.7); in cohort 3. Cohort 1 was significantly associated with longer PFS (adjusted HR: 0.53, 95% IC: 0.34–0.84, $p = 0.007$), and cohort 3 with shorter PFS (adjusted HR: 1.96, 95% IC: 1.21–3.15, $p = 0.006$) as compared to cohort 2. Exploratory analyses showed that HER2 spatial distribution predicted T-DXd response in patients with HER2-overexpressing mBC and that the transcriptomic response to T-DXd was different according to HER2 expression. No quantitative modulation of tumor microenvironment was observed after 6 to 8 weeks of treatment. Finally, recurrent mutations of the DNA repair gene *SLX4* were identified in 20% of samples at resistance (4/20) as compared to 2% in baseline samples (2/88), suggesting that *SLX4* mutations could mediate secondary resistance to T-DXd. These data suggest that HER2 is a key determinant of T-DXd efficacy. However, an antitumor activity is also observed in a subgroup of patients without detectable HER2 expression and resistance could be partially mediated by payload sensitivity.

Introduction

Breast cancer (BC) is the most commonly diagnosed cancer, with an estimated 2.3 million new cases per year, and the fifth leading cause of cancer mortality [1]. Despite advances of precision medicine and improvements in treatment, up to 30% of patients with early breast cancer will develop metastasis and 8% are diagnosed with *"de novo"* metastatic breast cancer (mBC), remaining incurable with a 5-year survival rate of 25%[2–4]. According to gene expression, BC includes three main subtypes namely hormone receptor-positive (HR-positive), HER2-overexpressing, and triple-negative breast cancer (TNBC)[5]. Antibody-drug conjugates (ADCs) are innovative drugs designed to deliver the cytotoxic payload to cells that express the target and thereby limiting potential systemic toxicity. Trastuzumab deruxtecan (T-DXd, DS-8201a) is a novel ADC composed of a humanized anti-HER2 monoclonal antibody, a cleavable tetrapeptide linker, and a novel topoisomerase I (TOP I) inhibitor as payload. T-DXd is characterized by a high drug-to-antibody ratio (DAR) of 8:1[6]. In DESTINY-breast01, a phase 2 single-arm study, T-DXd demonstrated high antitumor activity in patients with HER2- overexpressing mBC who received two or

more previous anti-HER2-based regimens in the metastatic setting[7]. In addition, T-DXd showed clinically meaningful improvement of progression-free survival (PFS) *vs.* ado-trastuzumab emtansine (T-DM1) in patients with HER2-overexpressing mBC (HR: 0.28, $p < 0.001$) in DESTINY-breast03, leading to regulatory approvals[8]. Finally, in DESTINY-breast04, a phase 3 randomized trial, T-DXd improved the median PFS (HR: 0.50, $p < 0.001$) and OS (HR: 0.64, $p = 0.001$) in patients with HER2-low mBC heavily pretreated[9].

Several questions are still unanswered. First, many aspects of the mechanism of action of T-DXd in patients remain unclear. Second, the mechanisms of resistance to T-DXd are unknown. In order to address these questions, we designed DAISY, a clinical trial that evaluates the efficacy of T-DXd in patients with mBC according to level of HER2 expression and explores treatment response and resistance through biomarker analyses on tumor samples at different timepoints.

Results

Study design and characteristics of the patients

Between November 2019 and March 2021, 186 patients with mBC whose disease progressed after ≥ 1 line of chemotherapy were included in DAISY trial. Cohort 1 included 72 patients with HER2-overexpressing mBC defined as IHC 3 + or IHC 2+/ISH-positive; cohort 2 included 74 patients with HER2-low mBC defined as IHC 2+/ISH-negative or IHC 1 + and cohort 3 included 40 patients with HER2 IHC 0 mBC (see methods for definition). Patients received T-DXd 5.4 mg/kg until progressive disease or unacceptable toxicity. The study design is displayed in Extended Data Fig. 1 and the CONSORT (Consolidated Standards of Reporting Trials) diagram in Extended Data Fig. 2. Patient's characteristics in the Safety Population ($n = 179$) are reported in Extended Data Table 1. Forty four patients (64.7%) in cohort 1, 58 (79.5%) in cohort 2, and 26 (68.4%) in cohort 3 had hormone receptor positive (HR-positive) BC. In total, 123 of 179 (68.7%) patients received previous endocrine therapy, including 108 (88.5%) who received at least one line in the metastatic setting. One hundred sixty two of 179 (90.5%) patients received previous targeted therapy, including 158 (98.1%) in the metastatic setting. Most of patients (53.1%) were heavily pretreated with ≥ 5 lines of previous chemotherapy.

Efficacy and safety results

The median number of cycles of T-DXd was 12.5 (range 2 to 31) in cohort 1, 10 (range 1 to 29) in cohort 2, and 6 (range 1 to 26) in cohort 3. In total, 145 patients (81%) permanently discontinued treatment, 49 (72.1%) in cohort 1, 61 (83.6%) in cohort 2 and 35 (92.1%) in cohort 3. The reason for discontinuation was disease progression in 125 (86.2%) patients and toxicity in 13 (9%) patients. Adverse events (AEs) are consistent with previous data[8] and are reported in Extended Data Tables 2 and 3. Three out of 179 (1.7%) patients presented AEs Grade 5. Nine out of 179 (5%) patients presented interstitial lung disease (ILD), all of them Grade 1/2, and five were reported by the investigator as treatment-related.

One hundred and seventy seven patients were included in the Full Analysis Set (Extended Data Fig. 2). As of the 19 October 2021 data cut-off, an objective response occurred in 93 (52.5%) patients including 86

with response confirmed: 48 patients (70.6%; 95% CI: 58.3–81) in cohort 1, 27 patients (37.5%; 95% CI: 26.4–49.7) in cohort 2, and 11 patients (29.7%; 95% CI: 15.9–47) in cohort 3 (Fig. 1a). The confirmed objective response was significantly different according to HER2 level expression across the three cohorts ($p < 0.0001$). In 93 patients with an objective response, the median duration of response (DoR) was 9.7 months (95%CI: 6.8–13) in cohort 1, 7.6 months (95%CI: 4.2–9.2) in cohort 2, and 6.8 months (95%CI: 2.8-not reached) in cohort 3. When we looked at the best tumor shrinkage of target lesions, we observed a median reduction of -57.2% (range: -100; 13.6), -25.3% (range: -100; 203.2), and − 12.5% (range: -80.6; 68.7) in cohort 1, 2, and 3 respectively ($p < 0.0001$). After a median follow up of 15.6 months (95% CI: 12.6–16.7), the median PFS was 11.1 months (95% CI: 8.5–14.4) in cohort 1, 6.7 months (95% CI: 4.4–8.3) in cohort 2, and 4.2 months (95% CI: 2.0-5.7) in cohort 3. Cohort 1 was significantly associated with longer PFS (adjusted HR: 0.53, 95% IC: 0.34–0.84, $p = 0.007$) and cohort 3 with shorter PFS (adjusted HR: 1.96, 95% IC: 1.21–3.15, $p = 0.006$) as compared to cohort 2 (exploratory analysis) (Fig. 1b). The confirmed objective response rate (ORR) and the median PFS were similar between patients with HER2 IHC 1 + and IHC 2+/ISH- in cohort 2 (Extended Data Fig. 3 and Fig. 4).

Association between HER2 expression patterns and treatment response

Since the clinical outcomes of the trial suggested that HER2 expression is a determinant of drug response, we further explore it in the cohort 1 (HER2 overexpressed) and cohort 3 (HER2 IHC 0). We first assessed whether HER2 spatial distribution predicts drug response in patients with HER2-overexpressing mBC. HER2 spatial distribution was defined by artificial intelligence (AI) in HER2 pathology slides at baseline in 61 patients with HER2 overexpressing mBC. Machine learning analyses using a clustering algorithm indicated that HER2 overexpressing slides could be decomposed into eight clusters (see Extended Data Fig. 6). Two clusters were associated with a different treatment response. A higher percentage of the surface of the slides presented cluster 6 in patients without an objective response ($p = 0.00057$) (Fig. 1c). Feature analyses identified that cluster 6 corresponded to a subset of HER2-negative areas with a low average cell density of 30%, containing mainly fibroblasts and immune cells (56% and 27% on average, respectively) and a vast majority of collagen fibers. For 28 out of 61 patients, it also comprised tumor cells, which were mainly scored 1 + and 0+, with a few cells scored 2 + and none 3+. On the other hand, the second cluster (cluster 4) was associated with an objective response ($p = 0.045$) (Fig. 1c). This cluster corresponded to a subset of HER2-stained areas showing strongly marked tumor cells (85% of tumor cells scored 3 + on average among all cells in this region), with a high average cell density of 96%.

We then assessed whether levels of HER2 expression could predict drug response in patients with HER2 IHC 0 mBC (cohort 3, $n = 37$). We first performed reverse transcription polymerase chain reaction (RT-PCR) for *ERBB2* gene expression in 24 FFPE tumor samples at baseline presenting ≥ 30% of tumor cells. Five out of 14 (35.7%; 95% CI: 12.8–64.9) patients with lower *ERBB2* gene expression presented a confirmed objective response as compared to three out of 10 patients (30%; 95% CI: 6.7–65.2) with higher *ERBB2* gene expression. Then, HER2 stained slides at baseline were reviewed by two pathologists for 31 patients

of cohort 3 (see Extended Data Fig. 8). Some level of HER2 expression were detected in 15 samples (8 “ultra-low” [defined in IHC section] and 7 IHC 1+). The confirmed objective response was observed in six out of 15 (40%; 95% CI: 16.3–67.7) patients *vs.* four out of 16 (25%; 95% CI: 7.3–52.4) patients with and without HER2 detection, respectively.

T-DXd mechanisms of action

We further explored T-DXd distribution in 10 paired metastatic lesions. As mentioned in the Methods section, the antibody used in these experiments recognizes Dxd. Nevertheless, the free-Dxd being washed during the IHC procedure, it’s unlikely that it is detected in these experiments. Five on-treatment biopsies were obtained on day 2–4 after cycle 1, one on day 7 after cycle 2, and one on day 1 of cycle 5 after infusion of T-DXd. Three pairs of biopsies were not analyzable because of the absence of cancer cells. As shown in Fig. 2a, tumor cells with a high level of HER2 expression presented greater T-DXd staining. At the opposite, three samples (two on day 2–4 after cycle 1 and one on day 1 of cycle 5) classified HER2 IHC0 by an enhanced protocol (see method) presented no or very few T-DXd staining (Pearson correlation coefficient $r = 0.75$, $p = 0.053$). Two of these three patients presented a confirmed partial response (PR) with a PFS of 17.8 (censored patient) and 12 months, respectively. In order to explore mechanisms of action of T-DXd, we analyzed the spatial differential gene expression between baseline and on treatment samples. Six HER2 IHC 0/IHC 1 + sample pairs at day 2–4 after Cycle 1 and two IHC2+/3 + at day 2 after cycle 2 and day 4–6 after cycle 3 were assessed. The analyses were performed using GeoMx technology and compared HER2-negative (HER2 IHC0) and HER2-overexpressing (HER2 IHC 3+) tumor area. Gene set enrichment analyses identified serotonin and G protein-coupled receptor signaling pathways enriched after T-DXd administration in HER2-overexpressing areas; and interferon alpha pathway in HER2-negative areas (Fig. 2b).

Modulation of tumor microenvironment

We then investigated whether T-DXd modulates the immune microenvironment. Thirty-one paired biopsies from a metastatic lesion at baseline and on day 22–43 after cycle 1 (18 from cohort 1, 10 from cohort 2, and three from cohort 3) were assessed by Multiplex fluorescent IHC. A significant decrease of PD-L1 expression in the cohort of patients with HER2 overexpressing mBC ($n = 18$; $p = 0.02$) was observed. Conversely, PD-L1 decrease was not observed in cohort 2 and 3. Furthermore, no quantitative modulation of immune cells by T-DXd was detected (Fig. 2c). Finally, the distance between immune and tumor cells did not decrease over T-DXd administration (data not shown).

Mechanisms of resistance to T-DXd

In order to identify potential mechanisms of resistance, we performed whole exome sequencing (WES) in biopsies obtained at baseline ($n = 88$) and at resistance ($n = 20$). Figure 3a reports the recurrent mutations and copy number at baseline, together with the sensitivity to T-DXd. No recurrent driver alterations were associated with upfront resistance. *ERBB2* hemizygous deletion was detected in five out of 88 (6%) patients at baseline. Interestingly, four of these patients did not respond to T-DXd (two cohort 2 and two cohort 3). We explored which genomic alterations were acquired at resistance by comparing the genomic

landscape of 10 pairs of pre- and post-treatment biopsies. As reported in Fig. 3a, 12 genes presented an alteration acquired at the time of resistance, in at least two out of 10 pairs. Interestingly, *SLX4* mutations were also observed in two additional post-treatment samples out of 10 post-treatment samples unmatched to pre-treatment. Overall four out of 20 samples obtained at the resistance to T-DXd presented a *SLX4* mutation (20%), as compared to 2% and 1% in pre-treatment and TCGA breast, respectively. To confirm that *SLX4* mutations might contribute to resistance to ADC armed with DXd, we assessed cell viability in two BC cell lines depleted for *SLX4* and treated with different doses of DXd for five days (Fig. 3b). We observed that *SLX4* loss leads to 5-20-fold increased resistance to high dose of DXd. This is reflected in the increase of inhibitory concentration (IC) 80 values after *SLX4* depletion i.e., 8.18 *vs* 167.27 nM and 95.1 *vs* 502.4 nM in SK-BR-3 and MCF-7 cells, respectively.

Finally, we investigated if HER2 expression and T-DXd distribution were modulated at the time of resistance. 13 out of 20 (65%, 95% CI: 40.8–84.6) patients presented a decrease of HER2 expression in the tumor, namely four IHC 3+ (two to IHC 2 + and two to HER 1+), five IHC 2+ (two to IHC 1 + and three to IHC 0), and four from IHC 1 + to IHC 0. Intratumoral distribution of T-DXd was observed in four out of six patients with a tumor biopsy collected at progression and ≤ 6 weeks after last infusion, suggesting that T-DXd can still be distributed to cancer cells in a subset of patients at resistance (Fig. 3c). Two of them presented HER2 IHC3 + at progression and the other two a decrease from HER2 IHC 3 + to 1+.

Discussion

In the present paper, we report converging evidence that the level of HER2 expression is a key determinant for the efficacy of T-DXd. Indeed, the PFS rates were significantly different across the three cohorts of patients, the percentage of HER2-overexpressing cells predicted efficacy in HER2-overexpressing tumors, the transcriptomic response to T-DXd was different according to HER2 levels and the levels of HER2 decreased at progression. While efficacy of first generation ADCs like T-DM1 was associated with target expression[10], this could not be found in last generation ADCs. Indeed, TROP2 expression was not predictive of Sacituzumab Govitecan efficacy in the ASCENT trial [11] and the efficacy of patritumab deruxtecan was observed across patients with mBC and a broad spectrum of HER3 expression[12,13]. Nevertheless, most of the patients included in the phase I/II trial testing patritumab deruxtecan in mBC presented high levels of HER3 tumor expression. While HER2 expression is the pillar for T-DXd sensitivity, DAISY provide evidence that a small subset of patients could present a durable objective response without evidence of HER2 detection or T-DXd uptake. The current study could not decipher the mechanism of action of T-DXd in these patients. Gene expression response to T-DXd suggests that interferon alpha pathway could be involved in sensitivity to T-DXd in HER2-negative areas, but it's unclear from this study whether this is a response to DNA damage or an antitumor effect mediated by immune cells[14].

In vivo data demonstrated an increase of PD-L1 expression in HER2-overexpressing colorectal cancer (CRC) cells in immunocompetent mouse models treated with T-DXd[15], which is the rationale to combine

T-DXd with immune checkpoint inhibitors (ICIs). In the present study, a decrease of PD-L1 expression was observed in HER2-overexpressing mBC treated with T-DXd due to the cytotoxic effect of this drug on tumor cells (n = 18). This could be explained by differences in the tumor microenvironment between animal and human models. Conversely, no quantitative modulation of immune cells was observed. Preclinical data reported an increase of tumor-infiltrating dendritic cells and CD8 + T cells in an immunocompetent mouse model with human HER2-overexpressing murine CRC cells treated with T-DXd, enhancing antitumor immunity and inducing immunogenic cell death[15–17]. Based on these data, several clinical trials assessing T-DXd in combination with ICIs are ongoing[18,19] Our study could not validate these findings, however there was no decrease of CD8 + T cells in contrast to previous observations after systemic chemotherapy alone[20]. Our results therefore suggest that the combination of ICIs plus T-DXd would have a stronger rationale as compared to ICIs plus systemic delivery of topoisomerase I inhibitors. Our analyses focused on quantitative changes of immune microenvironment, further analyses will focus on qualitative changes and activation of immune cells (perforin/granzyme).

In a case report, resistance to Sacituzumab Govitecan, an ADC targeting TROP2, was associated with TROP2 mutation and defective plasma membrane localization[21]. While HER2 expression substantially decreased at the time of resistance to T-DXd, there is no robust evidence that a reduction of T-DXd uptake is the dominant mechanism of resistance in the present study. Indeed, T-DXd was still distributed in the cancer cells in four out of six patients at the time of resistance. Unfortunately, no quantitative comparison of T-DXd uptake could be done during treatment and at resistance in these six patients. We also identified loss of function mutations of *SLX4* at progression in 4 patients (20%), results corroborated by *in vitro* analyses. *SLX4* encodes a DNA repair protein that regulates endonucleases, whose role in camptothecin resistance remains unclear[22]. In contrast to a previous report on Sacituzumab Govitecan[21], we could no detect *TOP1* mutations at the time of resistance.

The present study suggests that HER2 is a key determinant of sensitivity to T-DXd. Nevertheless, an antitumor activity is also observed in a small subset of patients whose cancer does not express HER2, suggesting that other mechanisms remain still uncover. Resistance mechanisms could involve multiple pathways (HER2 decrease, resistance to payload…), hinting that precision medicine approaches based on molecular analyses of cancer are necessary to develop drugs after resistance to T-DXd.

Patients And Methods

Patients and study design

DAISY (NCT04132960) is a prospective, phase II, open-label, clinical trial that assessed T-DXd efficacy in patients with mBC and performed biomarker analyses. The first patient was enrolled on 4th November 2019 and the last one on 3rd March 2021 at 15 study centers in France. The study design is reported in Extended Data Fig. 1. The first and last version of the protocol are displayed in Annex 1 and 2. Patients with mBC were eligible if they have received at least one line of chemotherapy in the metastatic setting,

have at least one non-bone metastatic site easily accessible to biopsy, and have signed the informed consent for biopsies throughout the study. Mandatory and optional tissue and blood biopsies performed during the study are described in the protocol (Annex 1 and 2). The biopsy at baseline could be skipped if a biopsy collected within 3 months before inclusion was available. Patients were assigned to three cohorts according to HER2 level expression determined by standard IHC, as previously reported[23], regardless HR status. Patients presenting HR-positive mBC had to be resistant to endocrine therapy plus CDK 4/6 inhibitors and patients with HER2 overexpressing mBC must be resistant to trastuzumab and ado T-DM1. DAISY trial was approved by the French ethics committee, CPP – Ile de France on September 05th 2019 and the French health authorities, ANSM, on July 08th 2019.

Treatments and follow-up

After signature of the informed consent and verification of all eligibility criteria, patients were treated with T-DXd intravenously 5.4 mg/kg every 3 weeks until disease progression or unacceptable toxicity, as defined by the investigator. Recommendations for dose reductions are described in the V1 of the protocol (Annex 1). Treatment efficacy was monitored by a computed tomography (CT) scan every 6 weeks during the initial 12 months and every 12 weeks thereafter. The CT-scan should be repeated at least 4 weeks after assessment of a partial response (PR) or a complete response (CR). The Response Evaluation Criteria in Solid Tumors (v1.1) were used to determine response and progression[24]. Toxicity data were collected at each visit and were classified according to the National Cancer Institute Common Terminology Criteria for Adverse Events (v5.0).

Immunohistochemistry (IHC)

ER, PR, and HER2 status were determined locally for screening. For cohort assignment, HER2 status determination on the baseline biopsy was performed within the GEFPICS pathologist network (national group of French pathologists experienced in breast cancer pathology, which publishes national breast cancer guidelines)[25]; i.e. each HER2 determination was mandatorily assessed by an expert breast cancer pathologist belonging to the GEFPICS' group. Centers that did not belong to the GEFPICS' group had therefore to send their sample to a member of this group, prior to cohort assignment. After HER2 central determination, thirteen and seventeen patients planned to be included in cohort 1 ($n = 72$) and 3 ($n = 40$) respectively, were included in cohort 2 ($n = 74$). Additionally, if HER2-expression from the biopsy at baseline was different from the status at screening, the patient was switched to the corresponding cohort (see Extended Data Fig. 8). ER and PR cut-off for positivity were set at 10% of tumor cells. HR status was determined on the primary tumor samples. HER2 status was defined according to the last version of the ASCO/CAP guidelines[23] and was determined on the primary tumor or metastases. "Ultra-low" HER2 category was defined as cases showing a faint to weak incomplete membrane staining in less than 10% of tumor cells (i.e. less than 1+, classified in the IHC 0 category following the ASCO/CAP guidelines[23]). HER2 staining was locally assessed in centers belonging to the GEFPICS' group using validated IHC protocols. All participating GEFPICS laboratories adhere to Assurance Quality programs dedicated to HER2 assessment in particular. HER2 staining on biopsies at progression was performed centrally at

Gustave Roussy using the 4B5 pre-diluted kit (VENTANA pathway HER2, clone: 4B5, Roche Diagnostics), according to the manufacturer's protocol.

Regarding T-DXd distribution, tissue sections were stained for HER2 with VENTANA anti-HER2/neu (4B5) Rabbit Monoclonal Primary Antibody (VENTANA pathway HER2, clone: 4B5, Roche Diagnostics) according to the manufacturer's instruction, and if necessary, the enhanced HER2 protocol was employed to detect low level of HER2 expression. For the enhanced HER2 protocol, OptiView DAB IHC Detection Kit (Roche Diagnostics) was used instead of ultraView Universal DAB Detection Kit (Roche Diagnostics). The percentage of tumor cells at each HER2 staining intensity was evaluated for HER2 score. HER2 was defined according to the last version of the ASCO/CAP guidelines[23]. In addition, tissue sections were stained for DXd-IgG using primary antibody against DXd (antiXAFG5737-1A3-ocChimera, Daiichi Sankyo) with Leica BOND RX automated slide stainer (Leica Biosystems). Rabbit isotype control antibody (#PA0777, Leica Biosystems) of equivalent concentration was used as negative reagent control. The DXd antibody was raised against a part of DXd and can recognize free DXd; however in FFPE samples, intracellularly cleaved free DXd is expected to be washed out during sample preparation and IHC procedure because DXd does not contain formaldehyde-sensitive group (ie, -NH2). The distribution and the percentage of DXd-IgG positive cells in total tumor cells was evaluated. Multiplex fluorescent IHC was performed with an Ultivue panel kit containing eight antibodies (2 times 4 barcoded markers) + Dapi. The antibodies to quantitatively analyze the immune and tumor cells and their spatial distribution were directed against CD3 (clone BC33), CD4 (clone SP35), CD8 (clone C8/144B), CD68 (clone KP-1), FoxP3 (clone 236A/E7), PD-1 (clone CAL20), PD-L1 (clone 73 – 10), PanCK/SOX10 (clone AE1/AE3/BC34). The cocktail of eight antibodies was applied at the beginning and fluorescent probes (complementary to each barcode label) were detected 4 by 4. Next, slides were stained for HES. After each detection cycle and HES staining, slides were imaged using the Akoya Biosciences PhenoImager HT (formerly Vectra Polaris). For each sample, the three Whole Slide Images (WSI) were stacked in one by Ultivue.

The resulting stacked WSI were analyzed in QuPath software. ROIs were manually delineated by a pathologist (MLT). Inside these regions, tissue was automatically detected using a trained classifier. Cells were detected on the Dapi channel and thresholding of each fluorescent channel allowed for phenotyping each cell, depending on the amount of signal present in the cell on each channel. Results were expressed, for each phenotype, as the number of stained cells per square millimeter of analyzed tissue. In addition, distance between each cell and the nearest CK + cell was computed. This allowed computation of the mean distance to CK for cells of each phenotype as well as a spatial distribution histogram of distance to CK of cells of each phenotype.

Assessment of HER2 spatial distribution by AI

Among the 68 patients from cohort 1, six patients with no digitized HER2 slide at baseline or not exploitable after pathologist review were removed. One patient presenting only one digitized HER2 slide at baseline scanned with another scanner was also moved away to ensure homogeneous scanning conditions (see Extended Data Fig. 8). Digitized HER2 IHC slides collected at baseline (n = 61) were

analyzed through an unsupervised scheme to identify homogeneous regions across patients, not relying on any prior assumptions linking specific tissue areas to objective response to treatment. These regions were segmented using a clustering algorithm on features extracted from pre-processed tissues; and region association to objective response was assessed through classic statistical analysis based on each cluster's relative percentage (see Extended Data Fig. 5).

A pathologist (IJG) first annotated regions of interest in the slides to discard biopsies without tumor tissue and tissue regions outside viable tumor. We contoured each tissue within these annotated areas using morphological operations. First, we down sampled the slides by a factor of 8 in each dimension to reduce image size and applied a grayscale conversion. We then subtracted the local average over a window size of from each pixel to retrieve an image near-zero mean, and computed the Law texture energy measures[26]. Finally, we applied a binary threshold on the spot texture map (above 20) with a flood fill algorithm to discard eventual remaining artifacts (blurry regions, ink stains) and extract final tissue contours. We isolated main tissues by enforcing a minimum area criterion (above 1500) to remove noisy elements introduced by the pre-processing. These contours were used to delimit the tissue from which patches were extracted. We chose a patch size of , without overlap, to carry the analysis at the level of a few cells and removed black and white patches by removing patches with over 70% of RGB values below 2 and 80% of RGB values above 250.

Following Lu et al.[27], we extracted 1024 visual appearance descriptors by applying a custom ResNet50 model pre-trained on ImageNet. We applied Mini-Batch K-Means[28] to extract clusters across all the slides from the patch descriptors, normalized by their mean and standard deviation. To determine the optimal number of clusters to construct, we computed the Davies-Bouldin Index from 2 to 15 clusters (Extended Data Fig. 6). Among the three highlighted local minima, only a decomposition of at least 8 clusters was considered sufficient to represent the heterogeneity in the slides[29], and so we selected this value. For each slide containing patches, we computed the cluster assignment of each patch using the trained clustering algorithm. We retrieved a vector of 8 features for each slide by counting the proportion of patches for each label :

$$V_i[k] = \frac{1}{N\_i} \sum_{n_i=1}^{N_i} 1_{\{L_{n_i}=k\}} \text{ for } k \in \{0 \dots 7\}$$

We used a Mann-Whitney U test to assess the statistical significance of each cluster percentage difference between positive and negative objective response. Finally, two pathologists (IJG, MLT) reviewed and annotated in details the cell content in cluster 4 and 6.

Reverse transcription polymerase chain reaction (RT-PCR)

To access of 18S, ACTB and HER2 expressions, 1µg RNA sample was reversed to into cDNA with SuperScript™ Vilo™ cDNA Synthesis Kit (ThermoScientific). Quantitative PCR was performed with

TaqMan™ Fast Advanced Master Mix using the TaqMan™ Gene expression Assays, respectively with Assays, Hs01111580 (HER2), Hs00197427 (ACTB) and HS99999901 (18S) as recommended from supplier (ThermoScientific). 18S and ACTB were used as an internal references to normalize input cDNA. The comparative threshold (△Ct) method was used. FFPE tumor samples were qualified for RT-PCR if ≥ 30% of the cells were tumor cells. The median of *ERBB2* relative expression was 30. The confirmed objective response according to *ERBB2* expression levels was calculated according to the median (> or ≤ median).

Digital Spatial Profiling (DSP)

FFPE tissue samples from eight patients profiled using GeoMx DSP at Gustave Roussy Cancer Center. For this experiment, 3-µm-thick FFPE slides from 1-week old were incubated with a multiplexed cocktail of primary RNA probes conjugated to unique oligonucleotide tags with an ultraviolet (UV) photocleavable linker. Tissue sections were imaged by three-color immunofluorescence using the morphological markers CD45, pan-cytokeratin (PanCK), and nuclear stain Syto13. For each slide, up to eight square ROI of 300 µm were drawn. No segmentation of the ROIs was performed. ROI placement was based on HER2 level expression and performed by a pathologist (MLT). An overlay of HER2 IHC slides images was done. ROI within the tissue were illuminated with UV light and oligo barcodes were physically aspirated from the tissue and collected into microtiter plates by the GeoMx® DSP platform. Each collection of oligo tags from one well (from the tissue section), was indexed using Illumina's index 1 (i7) and index 2 (i5) unique dual indexes system using GeoMx SeqCode primers with 18 cycles of PCR. After PCR, indexed ROIs were pooled and purified in two rounds of AMPure XP PCR purification using 1.2x bead:sample ratio. The resulting library fragments contain a unique molecular identifier (UMI), readout tag sequence identifier (RTS ID) that identifies the target, and the necessary regions for sequencing with Illumina platforms. GeoMx NGS libraries are sequenced with 2 x 27 bp paired-end reads using the unique dual index workflow with 8 bp for Index 1 (i7) and Index. The number of samples per sequencing run depends on the sequencing system and ROI size and number. Sequenced oligonucleotides are processed then imported back into the GeoMx DSP analysis software for integration with the slide image and ROI selections for spatially resolved RNA expression.

Genomic analyses

The tumor samples were qualified for genomic testing if ≥ 30% of the cells in the frozen sample were tumoral cells.

Genomic DNA was isolated from biopsy and blood of patients using the QIAamp® DNA Mini Kit and DNeasy® Blood and Tissue Kit (QIAgen), respectively, according to the manufacturer's guidelines. DNA samples were eluded in 21 µL of DNase-free water. DNA concentration was measured using QubitTM dsDNA Broad Range Assay (Invitrogen). A quantity of 30 to 100 ng of DNA was utilised for preparing the whole-exome sequencing libraries.

For the whole exome sequencing, the DNA was sheared with the Covaris E220 system (LGC Genomics / Kbioscience). SureSelect^{XT} Low Input Target Enrichment was used. Briefly, DNA fragments were end-repaired, extended with an 'A' base on the 3' end, ligated with paired-end adaptors with the Bravo Platform (Agilent Technologies) and amplified to generate libraries (ten cycles). Hybridization-based exome enrichment was performed using the Agilent SureSelect^{XT} Low Input Clinical Research Exome V2 target enrichment system (Agilent Technologies). The final libraries were indexed, pooled and sequenced using the onboard cluster method, as paired-end sequencing (2x100 bp reads) on Illumina NovaSeq-6000 sequencer at Gustave Roussy.

Bioinformatic analyses

Digital Spatial Profiling (DSP)

QCs were evaluated thanks to the manufacturer software (GeoMX DSP Control Center v2.4.2.2), all samples were kept. The raw count matrix was normalized by subtraction against the negative control probes provided by the manufacturer. Differential expression analyses (DEA) were performed using DESeq 2 (v1.36.0) under the R environment (v4.2.1), using default parameters. Selection of covariates to regress as sources of bias was performed by correlation- (continuous) or Kruskal-Wallis- (categorical covariates) tests against the first 10 components of a PCA performed on the normalized count matrix. Covariates with an coefficient above 0.5 in any of the 5 first PCs were used for regression during the differential test. GSEA analyses and plots were performed using clusterProfiler (v4.4.4) with the Gene Ontology and Reactome databases.

Genomic analyses

a. Point mutations and small indels - DAISY

Quality control of paired-end reads was accomplished using FastQC v0.11.8. Fastp v0.20[30] was subsequently employed for trimming adaptors and polynucleotide tracts from reads which were longer than 25 nucleotides. Afterwards, the resulting cleaned FASTQ files were aligned to the reference human genome GRCh37 using BWA-MEM v0.7.17[31]. Intermediate BAM files were further processed for deduplicating reads using MarkDuplicates from Picard v2.20.3, sorting coordinates using SAMtools v1.9[32], and finally recalibrating their base qualities using BaseRecalibrator and ApplyBQSR. All these tools are included in the GATK bundle v4.1.8.1[33]. Alignement quality was controlled using three different algorithms: mosdepth v0.2.5[34], flagstat from SAMtools v1.9[32], and CollectHsMetrics from GATK v4.1.8.1. Somatic point mutations and small indels were detected using Mutect2[35]. In order to remove artefacts and false-positives, a panel-of-normal was created from normal samples processed at Gustave Roussy using similar library preparation protocols and used at the Mutect2 calling step as specified in the GATK best practices. Putative variants were then analyzed for read orientation and sample contamination by running GATK LearnReadOrientationModel and CalculateContamination again as recommended in the

best practices. The following set of filters were applied: not filtered by Mutect2 (MUTECT_FILTERS), minimum VAF of 5% (LOW_VAF), minimum sequencing coverage of 20X in the tumor sample (LOW_COVERAGE_TUMOR), minimum sequencing coverage of 10X in the normal sample (LOW_COVERAGE_NORMAL), located inside exonic regions as defined by the set of canonical transcripts used by VEP v104 on GRCh37 assembly (NOT_EXONIC), allele frequency across all gnomAD v2.1 exome subpopulations is < 0.04% (COMMON_VARIANT). The last rule is not applied for variants annotated by OncoKB (see below) (Extended Data Fig. 7). A total of 16,238 somatic point mutations and small indels across 108 tumor/normal or tumor-only sample pairs (88 at baseline, 20 at resistance) were used for analysis.

b. Point mutations and small indels - TCGA-BRCA

Patients and samples attributes for TCGA study were downloaded from the GDC data portal using the R package GenomicDataCommons and from supplementary tables publicly available on the PanCanAltas page https://gdc.cancer.gov/about-data/publications/pancanatlas.

Point mutations and small indels for TCGA-BRCA were downloaded with permission from the file mc3.v.0.2.8.CONTROLLED.maf.gz[36].The file was first reduced to select only BRCA samples. Then the following set of filters was applied: minimum VAF of 5%; minimum sequencing coverage of 20X in the tumor sample; minimum sequencing coverage of 10X in the normal sample; located inside exonic regions as defined by the “Variant_Classification” column in the file mc3.v.0.2.8.CONTROLLED.maf.gz; for point mutations, select mutations seen by any 2 callers among the 5 callers used by MC3 (CENTERS column); for small indels, select indels seen by INDELOCATOR or VARSCANI among the 5 callers used by MC3 (CENTERS column). The filters were chosen in order to maximize the agreement between our Internal pipeline and MC3 pipeline. In short, 58 raw whole-exome sequencing files were downloaded with permission from the GDC data portal and processed using our internal pipeline. Applying the filters described above for DAISY mutation data and TCGA-BRCA mutation data, respectively, resulted in an overall dice-score index of 90% for point mutations and 84% for small indels. Most importantly, the burden was very similar (5,686 mutations on filtered MC3 table *vs.* 5,680 using raw sequencing files, 228 *vs.* 241 for indels). This comparison highlighted the excellent agreement between MC3-derived mutations and mutations identified using our internal pipeline.

c. Copy number alteration (CNA) - DAISY

Copy number alterations, tumor purity, and tumor average ploidy were identified with the FACETS R package v0.5.14[37] run with parameters cval_pre = 25 and cval_pro = 500. Lower-copy number (LCN) and total copy-number (TCN) are estimated by FACETS for each copy number segment identified. The ploidy of each segment in autosomes was normalized to the average tumor sample ploidy (TCNn = TCN/average ploidy) and categorized into 6 classes as following (similarly to what was done by Priestly et al[38]): LCN = 0, TCNn = 0: homozygous deletions (HomD); LCN = 0, TCNn < 0.6: hemizygous deletion (HemD); LCN = 0, 0.6 < TCNn < 1.4: copy-neutral loss of heterozygosity (cn-LOH); 1.4 < TCNn < 2: low-level

copy gain (LLG); 2 < TCNn < 3: middle-level copy gain (MLG); 3 < TCNn: high-level copy gain (HLG). Only HomD, MLG, and HLG on segments spanning less than 10 Mb were further considered.

d. Copy number alteration (CNA) – TCGA BRCA

Copy number alterations and average ploidy were downloaded from the publicly available files TCGA_mastercalls.abs_segtabs.fixed.txt and TCGA_mastercalls.abs_tables_JSedit.fixed.txt. These files were reduced to select only BRCA samples. The same categorization and filtering of CNAs as described in the previous paragraph was employed.

e. Catalogue of driver events

Oncogenic events were identified by intersecting point mutations and small indels that passed all filters as well as all HomD, MLG, and HLG spanning less 10 Mb with the OncoKB database[39]. Among the point mutations and indels that were annotated by oncokb-annotator, all events with MUTATION_EFFECT as “Likely Neutral”, “Neutral” or “Unknown” were discarded unless ONCOGENIC field was “Likely Oncogenic” or “Predicted Oncogenic”.

Experiment in BC cell lines

Cell culture

MCF-7 and SK-BR-3 cells were purchased from DSMZ (Germany). MCF-7 cells were grown in DMEM (Gibco) supplemented with 1% glutamax (Gibco) and SK-BR-3 in McCoy’s 5A medium (Gibco) in standard incubation conditions at 37°C with 5% CO_2. Both media were supplemented with 10% fetal bovine serum (FBS), penicillin (100 U/mL) and streptomycin (100 µg/mL) and cells. All cell lines were kept as mycoplasma-free.

Transfection

Cells were seeded at 5×10^3 cells/well in 96-well plate. Twenty-four hours later, cells were transfected with the siRNAs targeting *SLX4* gene (ON-TARGETplus siRNA – Smartpool, Dharmacon) or Non-targeting Control Pool (Dharmacon) using interferin according to the manufacturer’s instructions.

Cell viability

To evaluate cell viability, 48 h after siRNA transfection DXd was added with 8-point dose-response titrations in triplicate (0.1 nM – 1000 nM) for five days. Cell viability was examined using the CellTiter-Glo® Luminescent Cell Viability Assay (Promega) using VICTOR Nivo multimode plate reader (PerkinElmer). Survival at each drug concentration was calculated as a percentage relative to the corresponding untreated control.

Quantitative RT-PCR

To assess extinction of *SLX4* expression, total RNAs were extracted from cultured cells using RNeasy Minikit (Qiagen) and were reversed into cDNA with Maxima Reverse transcriptase (ThermoScientific). Quantitative PCR was performed with Master Mix PCR Power SYBR™ Green (Life Technologies) using CFX96™ Real Time System (Bio-Rad). The specific primers for *SLX4* used in this study were: 5'-GTGAAGGTCGGAGTCAACG-3' and 5'-GGTGAAGACGCCAGTGGACTC-3'. GAPDH was used as an internal reference to normalize input cDNA. The comparative threshold (△Ct) method was used.

Statistical analysis

Data were expressed as mean ± s.e.m. for $n = 3$. For viability assay, significance was analyzed by Welch's t-test (two-tailed). Statistical analysis was performed using GraphPad Prism 9 (GraphPad Software). *P*-values < 0.05 are considered statistically significant

Statistical analyses

The primary endpoint was the confirmed objective response rate evaluated using RECIST 1.1 criteria. The secondary endpoints include anti-tumour activity in each cohort in terms of progression-free survival (PFS) and duration of response (DoR) for patients presenting an objective response evaluated on the Full Analysis Set (FAS) and per cohort. Safety was evaluated on the safety population and per cohort. The required number of assessable patients for cohort 1 ($n = 67$) and 2 ($n = 40$) was determined using the A'Hern design with the following hypothesis: Cohort 1 (p0 = 30%; p1 = 45%, alpha = 5%, 1-beta = 80%) and Cohort 2 (p0 = 20%; p1 = 40%, alpha = 5%, 1-beta = 85%). The regimen would be declared promising in cohort 1 if 27 patients present a confirmed objective response among 67 and in cohort 2 if 13 confirmed objective response were observed among 40. Cohort 3 was designed using an optimal two stage design[40] (alpha = 5%, 1-beta = 85%) with non-progression at 3 months as short-term endpoint (p20 = 30% and p21 = 50%) and confirmed objective response as primary endpoint (p10 = 20%, p11 = 40%). A stop for non-promising activity was planned to be declared if four patients or less among the first 16 present non-progressive disease at 3 months. At final analysis of cohort 3, the regimen would be defined as promising if 13 patients or more present a confirmed objective response. For each cohort, it was assume a rate of 10% non-evaluable patients and sample size was increased: Cohort 1: $n = 74$, Cohort 2: $n = 44$, Cohort 3: $n = 44$. Full details are provided in statistical analysis plan.

The primary endpoint was described by cohort as number and percentage with corresponding 95% confidence interval and comparison between cohorts was performed using chi-square test. The best tumor shrinkage of target lesions was plotted on waterfall plot and compared between cohorts using the Kruskal-Wallis test. Time to event endpoints (PFS and DoR) were estimated using Kaplan-Meier method. Multivariable analysis was performed using Cox proportional hazards model adjusting for hormone receptor status of primary tumor (HR-positive *vs.* HR-negative), time from initial diagnosis to metastatic disease (0–3 months *vs.* >3 months), time from metastatic disease to inclusion (0–24 months *vs.* 24–60 months *vs.* >60 months), number of metastatic site (< 3 *vs.* ≥3 sites), presence of liver metastases and

ECOG performance status at inclusion. Hazard ratios were estimated with corresponding 95% confidence interval. In the exploratory analysis of modulation of tumor microenvironment, comparisons of each biomarker at baseline and on-treatment were performed using Wilcoxon matched-pairs signed-rank test. All statistical tests were two sided and no adjustment was made for multiple comparisons. Statistical analyses were carried out using Stata software v16 (StataCorp).

Declarations

Acknowledgements:

We acknowledge Tomoko Shibutani, Ryoto Yoshimoto and Hisashi Takahashi for pathology experiment and support.

References

1. Sung, H. *et al.* Global Cancer Statistics 2020: GLOBOCAN Estimates of Incidence and Mortality Worldwide for 36 Cancers in 185 Countries. *CA. Cancer J. Clin.* **71**, 209–249 (2021).

2. Cardoso, F. *et al.* 5th ESO-ESMO international consensus guidelines for advanced breast cancer (ABC 5). *Ann. Oncol. Off. J. Eur. Soc. Med. Oncol.* **31**, 1623–1649 (2020).

3. Malmgren, J. A., Mayer, M., Atwood, M. K. & Kaplan, H. G. Differential presentation and survival of de novo and recurrent metastatic breast cancer over time: 1990-2010. *Breast Cancer Res. Treat.* **167**, 579–590 (2018).

4. Grinda, T. *et al.* Evolution of overall survival and receipt of new therapies by subtype among 20 446 metastatic breast cancer patients in the 2008-2017 ESME cohort. *ESMO Open* **6**, 100114 (2021).

5. Comprehensive molecular portraits of human breast tumours. *Nature* **490**, (2012).

6. Ogitani, Y., Hagihara, K., Oitate, M., Naito, H. & Agatsuma, T. Bystander killing effect of DS-8201a, a novel anti-human epidermal growth factor receptor 2 antibody–drug conjugate, in tumors with human epidermal growth factor receptor 2 heterogeneity. *Cancer Sci.* **107**, 1039–1046 (2016).

7. Modi, S. *et al.* Abstract PD3-06: Updated results from DESTINY-breast01, a phase 2 trial of trastuzumab deruxtecan (T-DXd) in HER2 positive metastatic breast cancer. *Cancer Res.* **81**, PD3-06 (2021).

8. Cortés, J. *et al.* Trastuzumab Deruxtecan versus Trastuzumab Emtansine for Breast Cancer. *N. Engl. J. Med.* **386**, 1143–1154 (2022).

9. Modi, S. *et al.* Trastuzumab Deruxtecan in Previously Treated HER2-Low Advanced Breast Cancer. *N. Engl. J. Med.* **387**, 9–20 (2022).

10. Baselga, J. *et al.* Relationship between Tumor Biomarkers and Efficacy in EMILIA, a Phase III Study of Trastuzumab Emtansine in HER2-Positive Metastatic Breast Cancer. *Clin. Cancer Res. Off. J. Am. Assoc. Cancer Res.* **22**, 3755–3763 (2016).

11. Bardia, A. *et al.* Biomarker analyses in the phase III ASCENT study of sacituzumab govitecan versus chemotherapy in patients with metastatic triple-negative breast cancer . *Ann. Oncol.* **32**, 1148–1156 (2021).

12. Krop, Ian E. et al. Results from the phase 1/2 study of patritumab deruxtecan, a HER3-directed antibody-drug conjugate (ADC), in patients with HER3-expressing metastatic breast cancer (MBC). *J Clin Oncol 40, 2022 (suppl 16; abstr 1002)*.

13. Prat, A. et al. LBA3 - Patritumab deruxtecan (HER3-DXd) in early-stage HR+/HER2- breast cancer: final results of the SOLTI TOT-HER3 window of opportunity trial. *Annals of Oncology (2022) 33 (suppl_3): S165-S174. 10.1016/annonc/annonc890*.

14. Medrano, R. F. V., Hunger, A., Mendonça, S. A., Barbuto, J. A. M. & Strauss, B. E. Immunomodulatory and antitumor effects of type I interferons and their application in cancer therapy. *Oncotarget* **8**, 71249–71284 (2017).

15. Iwata, T. N. *et al.* A HER2-Targeting Antibody-Drug Conjugate, Trastuzumab Deruxtecan (DS-8201a), Enhances Antitumor Immunity in a Mouse Model. *Mol. Cancer Ther.* **17**, 1494–1503 (2018).

16. Gerber, H.-P., Sapra, P., Loganzo, F. & May, C. Combining antibody-drug conjugates and immune-mediated cancer therapy: What to expect? *Biochem. Pharmacol.* **102**, 1–6 (2016).

17. Nakajima, S. *et al.* The effects of T-DXd on the expression of HLA class I and chemokines CXCL9/10/11 in HER2-overexpressing gastric cancer cells. *Sci. Rep.* **11**, 16891 (2021).

18. Schmid, P. *et al.* BEGONIA: Phase 1b/2 study of durvalumab (D) combinations in locally advanced/metastatic triple-negative breast cancer (TNBC)—Initial results from arm 1, d+paclitaxel (P), and arm 6, d+trastuzumab deruxtecan (T-DXd). *J. Clin. Oncol.* **39**, 1023–1023 (2021).

19. Borghaei, H. *et al.* Trastuzumab deruxtecan (T-DXd; DS-8201) in combination with pembrolizumab in patients with advanced/metastatic breast or non-small cell lung cancer (NSCLC): A phase Ib, multicenter, study. *J. Clin. Oncol.* **38**, TPS1100–TPS1100 (2020).

20. Verma, R. *et al.* Lymphocyte depletion and repopulation after chemotherapy for primary breast cancer. *Breast Cancer Res.* **18**, 10 (2016).

21. Coates, J. T. *et al.* Parallel Genomic Alterations of Antigen and Payload Targets Mediate Polyclonal Acquired Clinical Resistance to Sacituzumab Govitecan in Triple-Negative Breast Cancer. *Cancer Discov.* **11**, 2436–2445 (2021).

22. Svendsen, J. M. *et al.* Mammalian BTBD12/SLX4 Assembles A Holliday Junction Resolvase and Is Required for DNA Repair. *Cell* **138**, 63–77 (2009).

23. Wolff, A. C. *et al.* Human Epidermal Growth Factor Receptor 2 Testing in Breast Cancer: American Society of Clinical Oncology/College of American Pathologists Clinical Practice Guideline Focused Update. *J. Clin. Oncol. Off. J. Am. Soc. Clin. Oncol.* **36**, 2105–2122 (2018).

24. Schwartz, L. H. *et al.* RECIST 1.1-Update and clarification: From the RECIST committee. *Eur. J. Cancer Oxf. Engl. 1990* **62**, 132–137 (2016).

25. Franchet, C. *et al.* [2021 update of the GEFPICS' recommendations for HER2 status assessment in invasive breast cancer in France]. *Ann. Pathol.* **41**, 507–520 (2021).

26. Laws, K. I. Textured Image Segmentation. *https://apps.dtic.mil/sti/citations/ADA083283* https://apps.dtic.mil/sti/citations/ADA083283 (1980).

27. Lu, M. Y. *et al.* Data-efficient and weakly supervised computational pathology on whole-slide images. *Nat. Biomed. Eng.* **5**, 555–570 (2021).

28. Pedregosa, F. *et al.* Scikit-learn: Machine Learning in Python. *J. Mach. Learn. Res.* **12**, 2825–2830 (2011).

29. Kalra, S. *et al.* Yottixel – An Image Search Engine for Large Archives of Histopathology Whole Slide Images. *Med. Image Anal.* **65**, 101757 (2020).

30. Chen, S., Zhou, Y., Chen, Y. & Gu, J. fastp: an ultra-fast all-in-one FASTQ preprocessor. *Bioinforma. Oxf. Engl.* **34**, i884–i890 (2018).

31. Li, H. & Durbin, R. Fast and accurate short read alignment with Burrows-Wheeler transform. *Bioinforma. Oxf. Engl.* **25**, 1754–1760 (2009).

32. Li, H. *et al.* The Sequence Alignment/Map format and SAMtools. *Bioinforma. Oxf. Engl.* **25**, 2078–2079 (2009).

33. DePristo, M. A. *et al.* A framework for variation discovery and genotyping using next-generation DNA sequencing data. *Nat. Genet.* **43**, 491–498 (2011).

34. Pedersen, B. S. & Quinlan, A. R. Mosdepth: quick coverage calculation for genomes and exomes. *Bioinforma. Oxf. Engl.* **34**, 867–868 (2018).

35. Cibulskis, K. *et al.* Sensitive detection of somatic point mutations in impure and heterogeneous cancer samples. *Nat. Biotechnol.* **31**, 213–219 (2013).

36. Ellrott, K. *et al.* Scalable Open Science Approach for Mutation Calling of Tumor Exomes Using Multiple Genomic Pipelines. *Cell Syst.* **6**, 271-281.e7 (2018).

37. Shen, R. & Seshan, V. E. FACETS: allele-specific copy number and clonal heterogeneity analysis tool for high-throughput DNA sequencing. *Nucleic Acids Res.* **44**, e131 (2016).

38. Priestley, P. *et al.* Pan-cancer whole-genome analyses of metastatic solid tumours. *Nature* **575**, 210–216 (2019).

39. Chakravarty, D. *et al.* OncoKB: A Precision Oncology Knowledge Base. *JCO Precis. Oncol.* **2017**, (2017).

40. Kunz, C. U., Wason, J. M. & Kieser, M. Two-stage phase II oncology designs using short-term endpoints for early stopping. *Stat. Methods Med. Res.* **26**, 1671–1683 (2017).

Figures

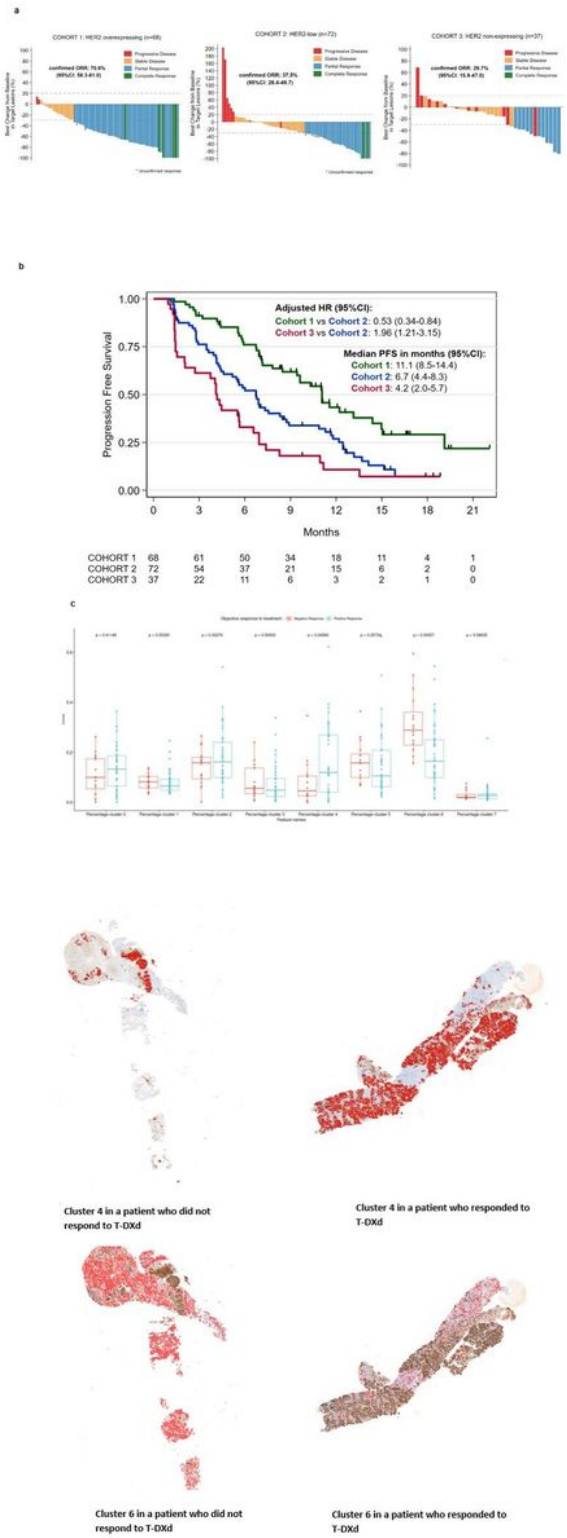

Figure 1

Efficacy of T-DXd and *association of HER2 expression patterns and treatment response*. a, Waterfall plot of the best change from baseline in target lesions according to the best objective response per cohort in the FAS population (*n*=177). The confirmed ORR with T-DXd of patients from cohort 1 (*n*=68) was 70.6% (95% CI: 58.3-81), from cohort 2 (*n*=72) was 37.5% (95% CI: 26.4-49.7), and from cohort 3 (*n*=37) was 29.7% (95% CI: 15.9-47). The difference of confirmed ORR was associated with HER2 level expression (*p*

<0.0001). *P*-value was calculated using Chi-square test. **b. Kaplan-Meier plot of PFS per cohort in the FAS population (*n*=177).**The median PFS was 11.1 months (95% CI: 8.5-14.4) in cohort 1, 6.7 months (95% CI: 4.4-8.3) in cohort 2, and 4.2 months (95% CI: 2.0-5.7) in cohort 3. The adjusted hazard ratio and *p*-value were derived from a multivariable Cox proportional hazard model taking as reference cohort 2 and adjusted for hormone receptor status, interval from initial diagnosis to metastatic disease, number and type of metastatic site, ECOG performance status and interval from metastatic disease to inclusion, was 0.53 (95% CI: 0.34-0.84); *p*=0.007 in cohort 1 and 1.96 (95% CI: 1.21-3.15); *p*=0.006 in cohort 3.**c. Clusters' relative percentage according to sensitivity to T-DXd.** For each patient, the corresponding slide was divided into 64 × 64 non-overlapping patches that were partitioned into 8 clusters using a Mini-Batch K-Means algorithm trained on all the slides. The following box plot illustrates the relative percentage of each of these cluster assignments among the patches for each patient. Two cluster highlights a significant difference between patients with a negative objective response (in red), and a positive one (in blue), namely cluster 6 and cluster 4, respectively. On the bottom, two pairs of pathology slides are reported. The first one reports area of Cluster 4 in red in a patient with resistance (left) or sensitivity (right) to T-DXd. Cluster 4 area represents HER2-stained areas with strongly marked tumor cells. The second one reports area of Cluster 6 in red in a patient with resistance (left) or sensitivity (right) to T-DXd. Cluster 6 area represents HER2-negative areas with a low average cell density, containing mainly fibroblasts and immune cells, and a vast majority of collagen fibers.

ORR: objective response rate; CI: confidence interval; T-DXd: Trastuzumab Deruxtecan; PFS: progression-free survival; HER2: HER2: Human Epidermal growth factor Receptor 2; FAS: Full Analysis Set

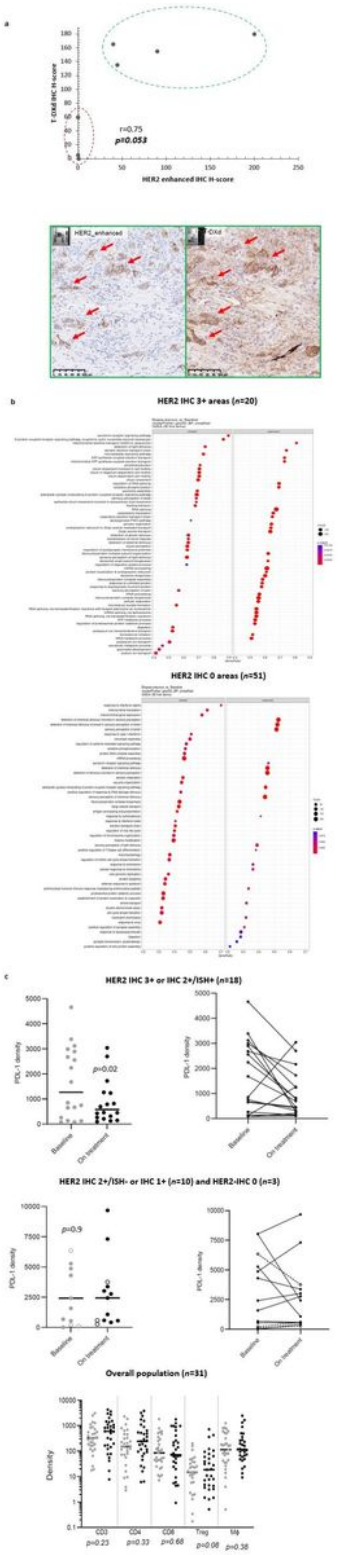

Figure 2

Differential mechanisms of action of T-DXd and modulation of tumor microenvironment. a. Illustration of the correlation between T-DXd distribution and HER2 expression. T-DXd was determined by IHC using an Ac anti DXd (H-score) and HER2 by an enhanced protocol of IHC (H-score) (*n*=7 sample pairs). The correlation was calculated by Pearson's correlation coefficient which showed a moderate correlation (*r*=0.75, *p*=0.053). On the bottom, a pathology slide that shows HER2 staining (red arrows) by an

enhanced protocol on the left and T-DXd staining (red arrows) by IHC on the right. **b. Spatial differential gene expression between baseline and on treatment samples.** Six HER2 IHC 0/IHC 1+ sample pairs at day 2-4 after Cycle 1 and two IHC 2+/3+ at day 2 after cycle 2 and day 4-6 after cycle 3 were assessed by GeoMx technology. Gene set enrichment analyses identified serotonin and G protein-coupled receptor signaling pathways enriched in HER2 IHC 3+ areas (*n*=20) and interferon alpha pathway in HER2 IHC 0 areas (*n*=51) after T-DXd administration. **c. Illustration of the modulation of the immune microenvironment by T-DXd by Multiplex Immunofluorescence (*n*=31).** Significant decrease of PD-L1 expression in FFPE biopsies performed on D22-43 after cycle 1 of T-DXd in patients with HER2 overexpressing mBC (*n*=18; *p*=0.02). At the opposite, no modification of PD-L1 expression in FFPE biopsies performed on D22-43 after cycle 1 of T-DXd in patients with HER2-low or HER2 non-expressing mBC (*n*=13; *p*=0.9). No quantitative modulation of the immune microenvironment by T-DXd in the overall population (*n*=31). Grey bullets and black ones represents at baseline and on-treatment samples, respectively. *P*-value was calculated using the Wilcoxon matched-pairs signed-rank test.

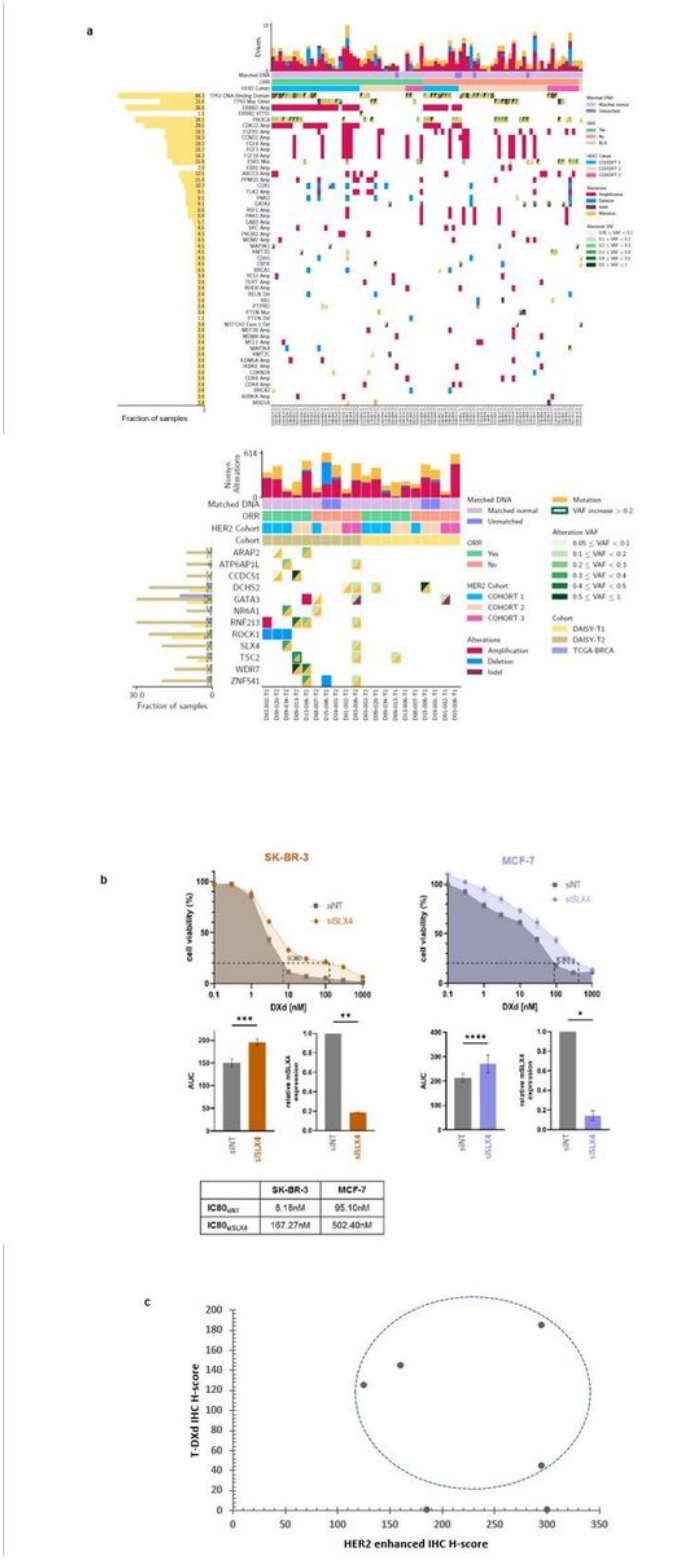

Figure 3

Mechanism of resistance to T-DXd. a. Oncoplot of driver mutations and copy number alterations (Oncokb + CIViC) identified in at least 3% of biopsies at baseline (T1, *n*=88). If a gene has at least one driver mutation in at least 3% of T1 biopsies, each other driver alteration of the same gene regardless of the frequency is shown. **Oncoplot of genomic alterations identified in at least two biopsies at progression (T2).** Ten T2 biopsies (progression) were matched with biopsies at baseline (T1). The genomic alterations

observed in at least two samples at resistance are reported in the oncoplot (*n*=10 pairs). In addition, the histogram on the left side of the oncoplot reports the frequency of alterations observed in the overall 20 samples obtained at resistance (10 matched to T1 and 10 unmatched to pre-treatment samples). The cut-off for the amplifications was determined at 3. **b. Dose–response survival curves of SK-BR-3 and MCF-7 cells transfected with non-targeting or SLX4-targeted siRNAs and exposed to DXd at the indicated doses for five days.** AUC and IC80 were determined for each condition. Data are mean surviving fractions ± s.e.m., $n = 3$. $*P < 0.05$, $**P < 0.01$, and $***P < 0.001$. Statistical analysis was performed using Welch's t-test (two-tailed). AUC: area under the curve. **c. Illustration of T-DXd uptake and HER2 expression at progression (*n*=6).** T-DXd was determined by IHC using an Ac anti DXd (H-score) and HER2 by an enhanced protocol of IHC (H-score). T-DXd was observed in four of six patients whose biopsy at progression was done ≤6 weeks after last infusion.

Supplementary Files

This is a list of supplementary files associated with this preprint. Click to download.

- ExtendedfiguresDAISY2022.09.18.docx
- ExtendedtablesDAISY2022.09.18docx.docx
- 190712ProtocoleDAISYV1.1vfsignXX.pdf
- 210125ProtocoleDAISYV3.0finalcleansignXX.pdf
- DAISYsapv1.020210908vffullsigned.pdf
- flatAndreepc.pdf
- flatAndrers.pdf